Electronic Supplementary Material (ESI) for Journal of Materials Chemistry A.

Supporting Information For:

Unraveling the device performance differences between bulk-heterojunction and single-component polymer solar cells

Yina Zheng,[1] Yao Wu,[1] Zhihao Chen,[2] Xinxin Xia,[3] Yawen Li,[4] Qiang Wu,[1] Yuze Lin,[4] Xinhui Lu,[3] Xiaotao Hao,[2] Jie Min[1]*

[1]The Institute for Advanced Studies, Wuhan University, Wuhan 430072, China
E-mail: min.jie@whu.edu.cn

[2]School of Physics, State Key Laboratory of Crystal Materials, Shandong University, Jinan, Shandong, 250100 P. R. China

[3]Department of Physics, Chinese University of Hong Kong, New Territories, Hong Kong 999077, China

[4]Beijing National Laboratory for Molecular Sciences, CAS Key Laboratory of Organic Solids, Institute of Chemistry, Chinese Academy of Sciences, Beijing, 100190, China

1. Experimental Section

1.1. Materials

PBDB-T, F3N, IC-BrCl-1 and IC-BrCl-2 were purchased from Solarmer Materials Inc (molecular structure were illustrated at Scheme S1). Yao Wu synthesized the PYCl-2 and PBDB-YTCl-2 materials and the synthesis routes were illustrated at Scheme S2. Chloroform (CF) were dried and distilled from appropriate drying agents prior to use. The processes of the purification of CF are as followed: The purifications involve washing with water for several times to remove the ethanol, drying with potassium carbonate, refluxing with calcium chloride, and then distilling. The distilled CF were stored in the dark to avoid the photochemical formation of phosgene.

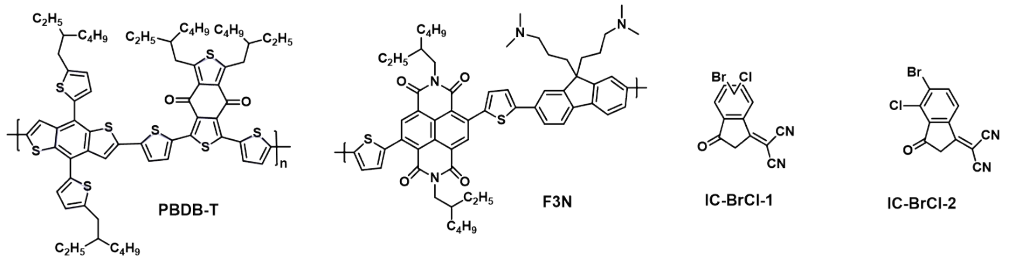

Scheme S1. Molecular structure of PBDB-T, F3N, IC-BrCl-1 and IC-BrCl-2.

Synthesis of YC20-Cl-2

Y5C20-CHO (1g, 0.73 mmol), IC-BrCl-1 (338 mg, 1.1 mmol), IC-BrCl-2 (338 mg, 1.1 mmol), chloroform (100 mL) were added to a single-necked round-bottomed flask under nitrogen, followed by pyridine (1 mL) dropwise. The mixture was stirred at 50 °C overnight. After cooling to room temperature, the mixture was poured into methanol (250 mL) and filtered. The residue was purified by column chromatography on silica gel using chloroform/petroleum ether (2:1) as eluent, yielding a dark blue solid (673 mg, 47.3%). ^{1}HNMR (600 M, $CDCl_3$) δ 9.12 (s, 1H), δ 9.09 (s, 1H), 8.87 (s, 0.5H), 8.68 (s, 0.5H), 8.45 (d, 1H, J = 8.28 Hz), 8.06 (s, 0.5H), 7.90 (d, 1H, J = 8.28 Hz), 7.87 (s, 0.5H), 4.71 (t, 4H, J = 6.36 Hz), 3.14 (t, 4H, J = 6.6 Hz), 2.04-2.07 (m, 2H), 1.77-1.82 (m, 4H), 1.42-1.47 (m, 4H), 1.29-1.31 (m, 4H), 0.91-1.21 (m, 88H), 0.80 (t, 6H, J = 6.81 Hz), 0.76 (t, 6H, J = 7.2 Hz), 0.70-0.73 (m, 6H).

Synthesis of PYCl-2 (poly[(2,2'-((2Z,2'Z)-((12,13-bis(2-octyl dodecyl)-3,9-diundecyl-12,13-dihydro[1,2,5]thiadiazolo[3,4e]thieno[2",3":4',5']thieno[2',3':4,5]pyrrolo[3,2-g]thieno[2',3':4,5]thieno[3,2-b]-indole-2,10-diyl)bis(methanylylidene))bis(3-oxo-2,3-dihydro-1H-indene-2,1-diylidene))dimalononitrile-alt-2,5-thiophene)]: YC20-Cl-2 (150g, 0.077 mmol) and 2, 5-bis (trimethylstannyl) thiophene (31.6 mg, 0.077 mmol) were dissolved in 10 ml anhydrous toluene in a two-necked flask. $Pd(PPh_3)_4$ (4.5 mg, 0.004 mmol) was added into the mixtures after being flushed with argon for 30 minutes. The reactions were stirred at 110 °C for 2 h. After cooling to room temperature, the mixture was poured into methanol and filtered. Then it was subjected to Soxhlet extractions with methanol, hexane, acetone, and chloroform each for 24 hours, respectively. Then the chloroform fraction was concentrated and precipitated with methanol. After vacuum drying at 45 °C for 12 h, the black solid was obtained with a yield of about 85%.

Synthesis of PBDB-YTCl-2

D1 (135 mg, 0.144 mmol) and A1 (110.1 mg, 0.144 mmol) were dissolved in 10 ml of anhydrous toluene in a two-necked flask. The mixture was deoxygenated with nitrogen for 30 min and then the catalyst $Pd(PPh_3)_4$ (16 mg, 0.014 mmol) was added. The reactions were stirred at 110 °C for 4 h. Then D2 (58.8mg, 0.144mmol) and YC20-Cl-2 (278.9mg, 0.144mmol) were dissolved in 10 mL toluene and added into the reaction system through a syringe with stirring at 110 °C for another 2 h. After cooling to room temperature, the mixture was poured into methanol and filtered. Then it was subjected to Soxhlet extractions with methanol, hexane, acetone, and chloroform each for 24 hours, respectively. Then the chloroform fraction was concentrated and precipitated with methanol. After vacuum drying at 45 °C for 12 h, the black solid was obtained with a yield of about 80%.

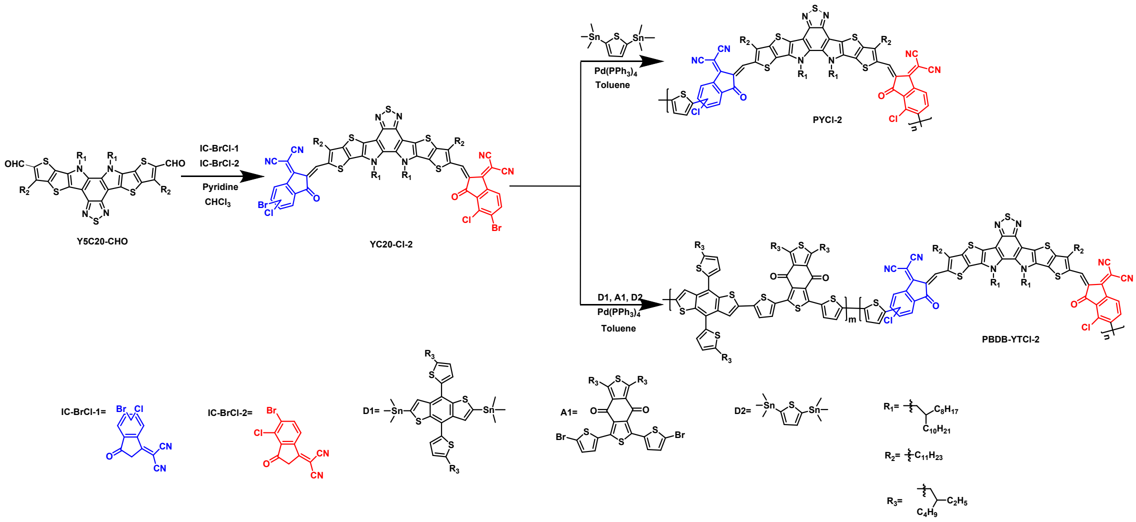

Scheme S2. Synthesis routes of the polymer acceptor PYCl-2 and the single-component system PBDB-YTCl-2.

1.2. Device Fabrication and Testing

***Solar cell devices fabrication*:** The solar cell devices were fabricated with a conventional structure of Glass/ITO/PEDOT: PSS (40 nm)/Active Layer/F3N (30 nm)/Ag (100 nm). Pre-patterned ITO coated glass substrates washed with methylbenzene, deionized water, acetone, and isopropyl alcohol in an ultrasonic bath for 15 minutes each. After blow-drying with high-purity nitrogen, all ITO substrates are cleaned in the ultraviolet ozone cleaning system for 15 minutes. Subsequently, a thin layer of PEDOT: PSS was deposited through spin-coating on pre-cleaned ITO-coated glass at 5000 rpm for 20 s and dried subsequently at 150 °C for 15 minutes in atmospheric air. The photovoltaic layers were spin-coated in a glovebox. The PBDB-T:PYCl-2 (1:1, wt%) BHJ blend and PBDB-YTCl-2 SC solution were prepared using chloroform solvent with 18 mg/ml and 4% CN by volume as additive. The BHJ and SC active layers were fabricated by spin-coating at about 3000rpm for the 30s and then thermal annealing at 100 ℃ for 10 mins. The thickness optimal active layer measured by a Bruker Dektak XT stylus profilometer was about 100 nm. A F3N layer *via* a solution concentration of 1 mg mL^{-1} was deposited at the top of the active layer at a rate of 3500 rpm for 20 s. Finally, the top argentum electrode of 100 nm thickness was thermally evaporated through a mask onto the cathode buffer layer under a vacuum of ~ 5×10^{-6} mbar. The typical active area of the investigated devices was 5 mm^2. The current-voltage characteristics of the solar cells were measured by a Keithley 2400 source meter unit under AM1.5G (100 mW cm^{-2}) irradiation from a solar simulator (Enlitech model SS-F5-3A). Solar simulator illumination intensity was determined at 100 mW cm^{-2} using a monocrystalline silicon reference cell with a KG5 filter. Short circuit currents under AM1.5G (100 mW cm^{-2}) conditions were estimated from the spectral response and convolution with the solar spectrum. The forward scan was adopted to test the J-V curves, and the scan step is 0.02 V and the delay time is 1 ms. The scan mode is sweep. The external quantum efficiency was measured by a Solar Cell Spectral Response Measurement System QE-R3011(Enli Technology Co., Ltd.).

1.3. Instruments and Characterization

Gel permeation chromatography (GPC) measurement**:** Molecular weight of the polymers was measured using a high-temperature gel permeation chromatography (GPC, Agilent PL-GPC220) at 145 °C with 1,2,4-trichlorobenzene as the eluent and polystyrenes as the standards.

Electrochemical characterizations**:** Cyclic voltammetry was carried out on a CHI610E electrochemical workstation with three electrodes configuration, using Ag/AgCl as the reference electrode, a Pt plate as the counter electrode, and a glassy carbon as the working electrode. 0.1 mol L^{-1} tetrabutylammonium hexafluorophosphate in anhydrous acetonitrile was used as the supporting electrolyte. The polymer and small molecules were drop-cast onto the glassy carbon electrode from chloroform solutions (5 mg/mL) to form thin films. Potentials were referenced to the ferrocenium/ferrocene couple by using ferrocene as external standards in acetonitrile solutions. The scan rate is 100 mV s^{-1}.

Optical measurements and simulations**:** Ultra-violet-visible near-infrared (UV-vis-NIR) absorption spectra were recorded with a Perkin-Elmer Lambda 365 UV-Vis spectrophotometer from 300 nm to 1100 nm. The optical simulations were calculated by Fluxim Setfos software.

Grazing incidence wide-angle and small-angle X-ray scattering (GIWAXS and GISAXS) characterization**:** The grazing incidence X-ray scattering (GIWAXS) measurement was carried out with a Xeuss 2.0 SAXS/WAXS laboratory beamline using a Cu X-ray source (8.05 keV, 1.54 Å) and a Pilatus3R 300K detector. The incident angle was 0.20°. The samples for GIWAXS/GISAXS measurements were fabricated on silicon substrates.

Transient absorption spectroscopy (TAS)**:** For femtosecond transient absorption spectroscopy, the fundamental output from Yb: KGW laser (1030 nm, 220 fs Gaussian fit, 100 kHz, Light Conversion Ltd) was separated to two light beams. One was introduced to NOPA (ORPHEUS-N, Light Conversion Ltd) to produce a certain wavelength for the pump beam (450nm/800 nm, below 7.5 μJ/cm^2 pulse, 100 fs pulse duration), and the other was focused onto a YAG plate to generate white light continuum as the probe beam. The pump and probe overlapped on the sample at a small angle less than 10°. The transmitted probe light from the sample was collected by a linear CCD array.

Photoluminescence (PL) and Electroluminescence (EL) measurements: The PL data and emission of relevant films were collected using a Zolix Flex One Spectrometer. For the film samples, the PL excitation wavelength was set to 639 nm. The EL signature was collected with a monochromator and detected with an InGaAs detector.

***Photo-induced charge carrier extraction by linearly increasing the voltage (photo-CELIV) measurements*:** In photo-CELIV measurements, the devices were illuminated with a 405 nm laser diode. Current transients were recorded across the internal 50 Ω resistor of our oscilloscope. Here, a fast electrical switch was used to isolate the device in order to prevent carrier extraction or sweep out. After the variable delay time, the switch connected the device to a function generator. It applied a linear extraction ramp, which was 40 μs long and 2.0 V high. Moreover, it started with an offset matching the V_{OC} of the device for each delay time. To determine the mobility in the devices, photo-CELIV curves were measured using different experimental conditions, differing in delay time and applied voltage.

***Space charge limited current (SCLC) measurements*:** Single carrier devices were fabricated and the dark current-voltage characteristics were measured and analyzed in the space charge limited (SCL) regime following the references. The structure of hole-only devices was Glass/ITO/PEDOT:PSS/Active Layer/MoO_3 (10nm)/Ag (100 nm). For the electron-only devices, the structure was Glass/ITO/ZnO/Active Layer/F3N/Ag (100 nm), where the Ag was evaporated. The *J*-*V* characteristics of both hole-only and electron-only diodes can be excellently fit the Mott-Gurney relation for space charge limited current

$$J_{SCL} = \frac{9}{8}\varepsilon_0\varepsilon_r\mu\frac{V_{in}^2}{L^3}exp(\frac{0.89 \times \beta}{\sqrt{L}}\sqrt{V_{in}}), \quad (1)$$

Where J_{SCL} is the current density, ε_0 is the permittivity of free space, ε_r is the relative dielectric constant of the active layer, μ is the charge carrier mobility, β is the field activation factor, L is the thickness of the device and V_{in} is the voltage dropped across the sample.

Fourier-transform photocurrent spectroscopy external quantum efficiency (FTPS-EQE)**:** FTPS-EQE measurement was performed at a Vertex 70 from Bruker Optics, which is equipped with a quartz tungsten halogen lamp, quartz beam-splitter, and external detector option. The amplification of the photocurrent product was achieved by using a low-noise current amplifier (SR570) on the illumination of the photovoltaic devices with light modulated by the Fourier transform infrared spectroscopy (FTIR). The external detector port of the FTIR gathered the signals from the current amplifier for output voltage. A Keithley 2400 SourceMeter was used for supplying voltages and recording injected current, and a Keithley 485 picoammeter was used for measuring the emitted light intensity.

Trap density of states (tDOS)**:** tDOS were performed on Keysight 4980A and analyzed by using the thermal admittance spectroscopy method.[1] The BHJ and SC devices used for the thermal admittance spectroscopy measurements were encapsulated and have the same structure with the device optimized in this work: Glass/ITO/PEDOT: PSS /Active Layer/F3N/Ag. The angular frequency-dependent capacitance can derive the energetic profile of tDOS of solar cells according to the following equation[2]

$$N_T(E_\omega) = -\frac{V_{bi}\, dC \;\; \omega}{qW d\omega k_B T}, \quad (2)$$

where k_{B} is the Boltzmann's constant, ω is the angular frequency, C is the capacitance,

T is the absolute temperature, W is the depletion width, and V_{bi} is the built-in potential. The applied angular frequency ω is defined by the following formula[2]

$$E_{\omega} = k_B T ln(\frac{\omega_0}{\omega}), \tag{3}$$

where ω_0 is the attempt-to-escape frequency. The trap states below the energy demarcation can capture or emit charges with the given ω and contribute to the capacitance.

2. Supplementary Figures and Tables

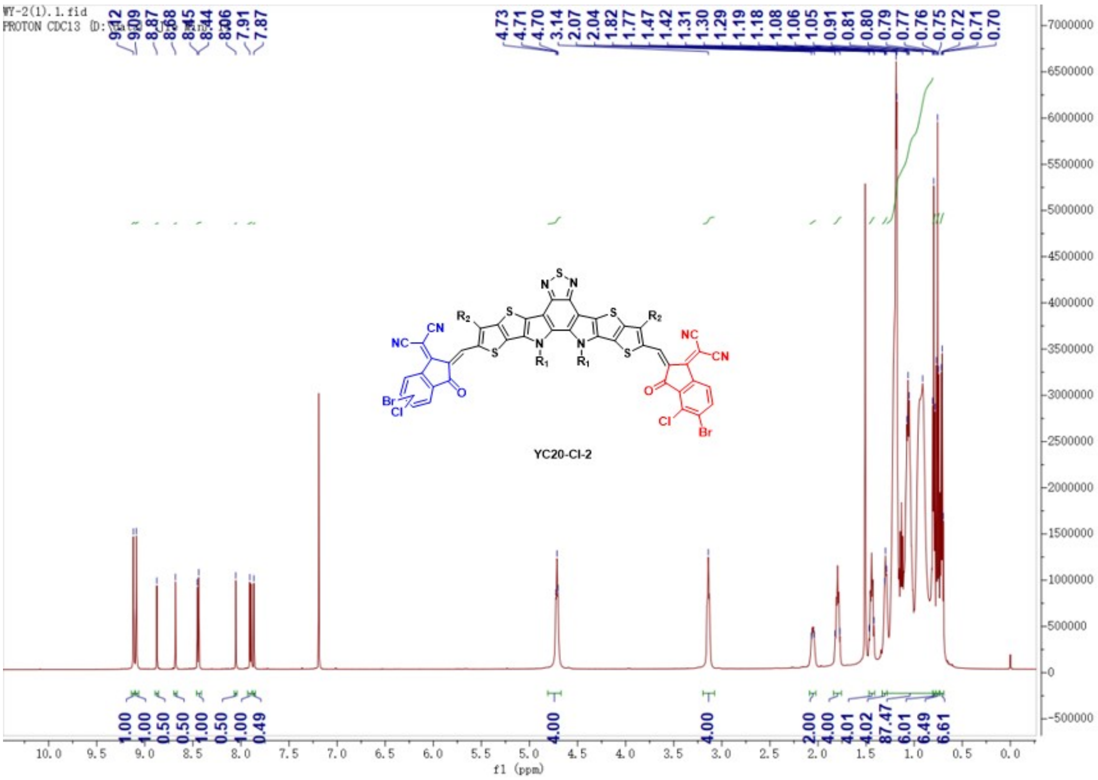

Figures S1. ^{1}HNMR spectrum of Y20-Cl-2 (600 MHz, $CDCl_3$).

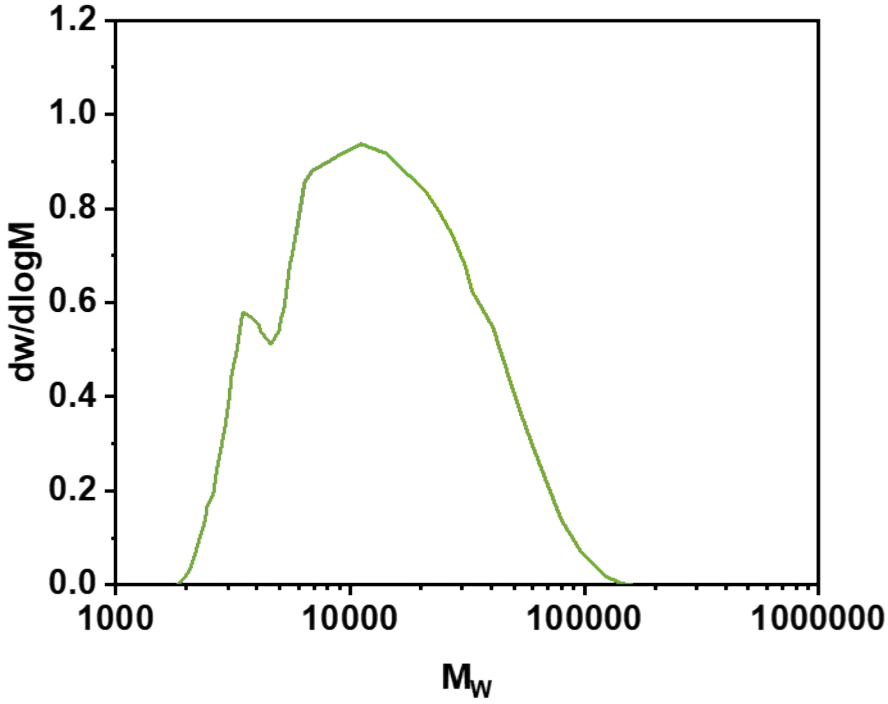

Figure S2. GPC curve of polymer acceptor PYCl-2.

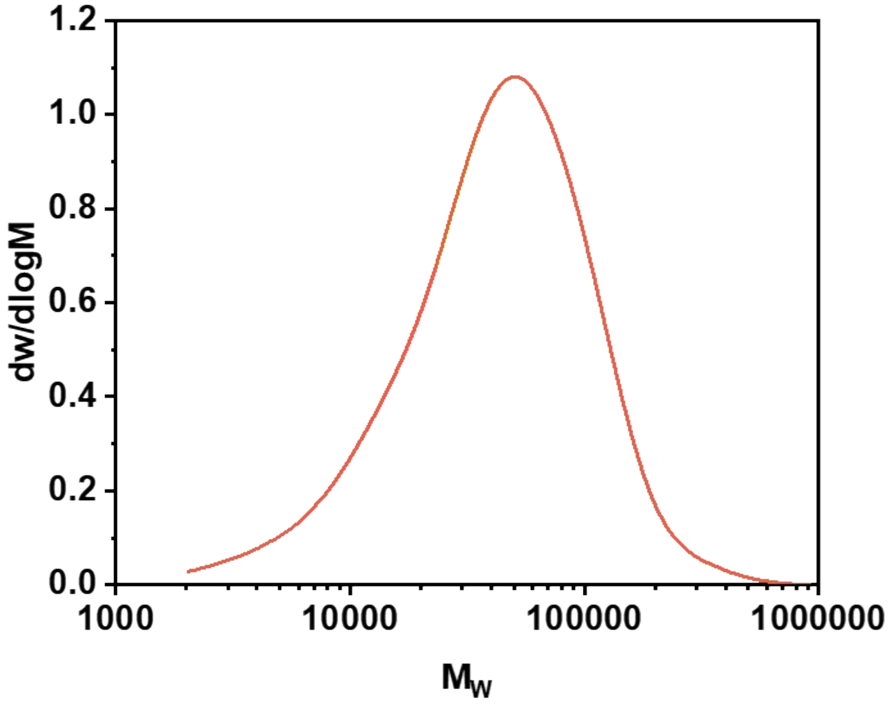

Figure S3. GPC curve of PBDB-YTCl-2.

Table S1. Molecular weight, optical and electrochemical properties of PBDB-T, PYCl-2 and PBDB-YTCl-2.

Sample	M_n [kDa]	M_w [kDa]	PDI	λ_{max} [nm][a]	λ_{max} [nm][b]	λ_{onset} [nm][b]	E_g^{opt} [eV][c]	HOMO/LUMO [eV][d]
PBDB-T	/	/	/	620	628	685	1.81	-5.33/-3.52[e]
PYCl-2	8.96	18.2	2.03	749	816	896	1.38	-5.71/-3.86
PBDB-YTCl-2	24.4	59.8	2.45	759	807	889	1.39	-5.53/-3.65

[a]Measured from the dilute $CHCl_3$ solutions. [b]Measured from films on quartz cast from $CHCl_3$ solution. [c]Calculated from the empirical formula: $E_g^{opt} = 1240/\lambda_{onset}$. [d]Obtained from the cyclic voltammetry (CV) method unless otherwise stated. [e]The LUMO level was calculated from $E_{LUMO} = E_{HOMO} + E_g^{opt}$, because the reduction peak of PBDB-T is too smooth to obtain the exact LUMO level.

Table S2. Elemental analysis data of PBDB-T-YTCl-2.

Sample	Element	Unit	Result	Method
PBDB-T-YTCl-2	N	%	3.48	CHNS
	C	%	70.05	CHNS
	H	%	6.958	CHNS
	S	%	13.507	CHNS

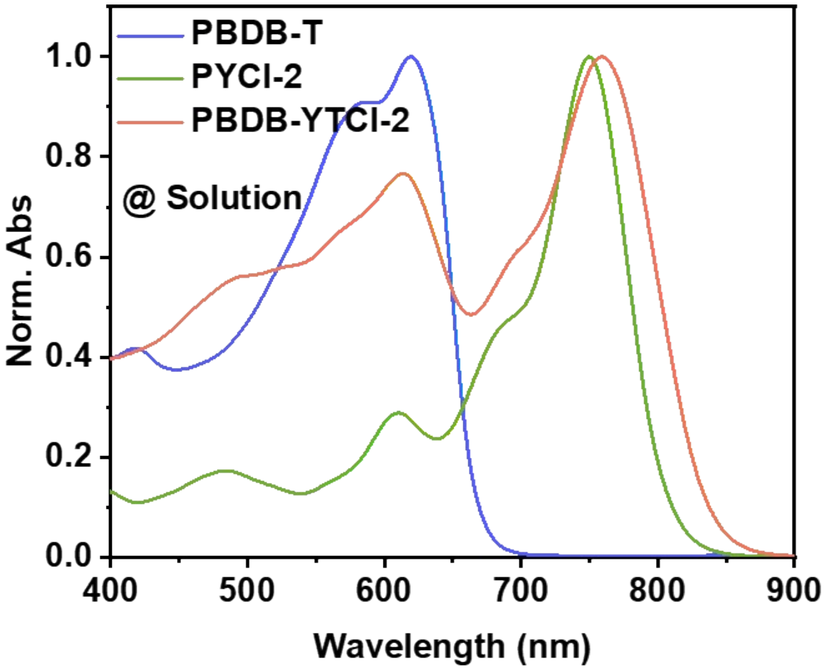

Figure S4. The ultraviolet-visible near-infrared (UV-*vis*-NIR) of the PBDB-T, PYCl-2 and PBDB-YTCl-2 in chloroform solutions.

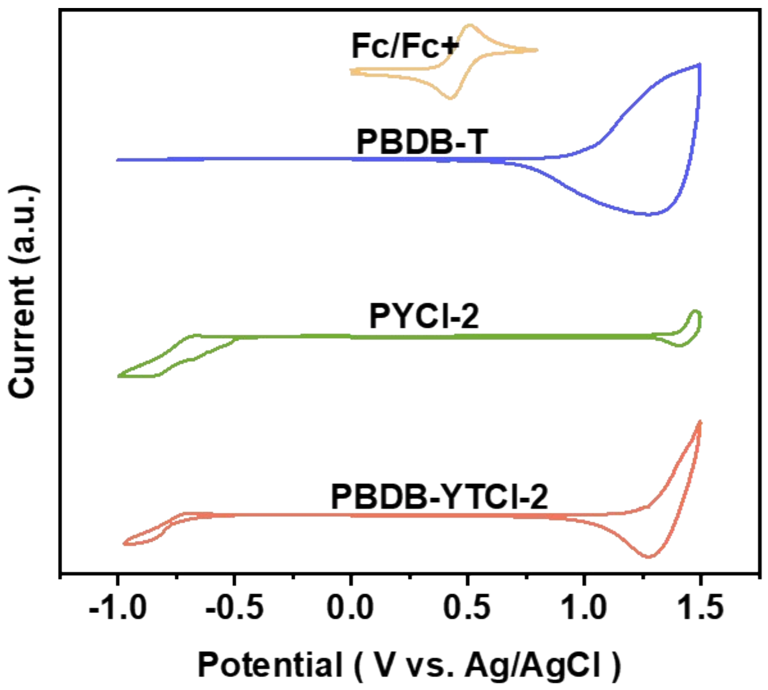

Figure S5. Cyclic voltammetry curves of PBDB-T, PYCl-2 and PBDB-YTCl-2.

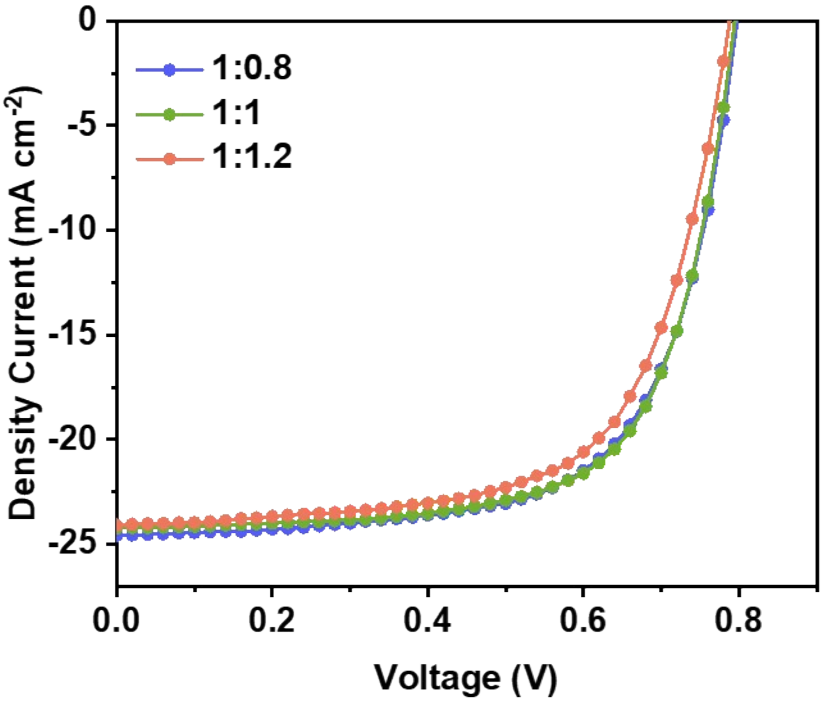

Figure S6. *J-V* curves of the BHJ devices with different D/A ratios, measured under one sun illumination.

Table S3. Photovoltaic parameters of the BHJ devices with different D/A ratios, measured under one sun illumination

D:A ratio	PCE [%]	FF [%]	V_{OC} [V]	J_{SC} [mA cm^{-2}]
1:0.8	12.96	66.14	0.797	24.58
1:1	13.09	68.00	0.795	24.23
1:1.2	12.35	65.06	0.788	24.10

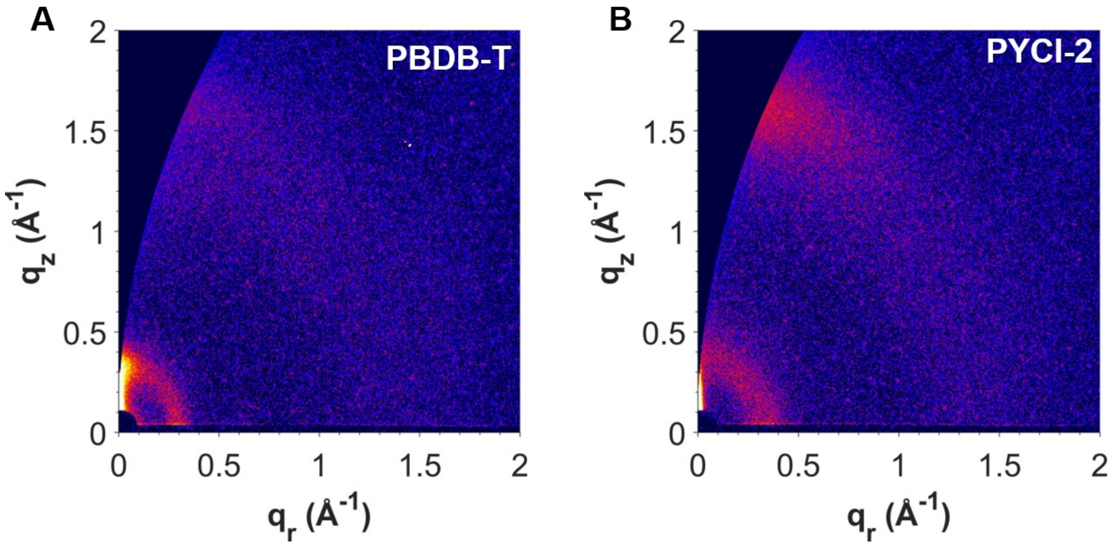

Figure S7. GIWAXS patterns of (A) PBDB-T and (B) PYCl-2 films.

Table S4. Investigations of the morphology parameters extracted from the GIWAXS measurements of PBDB-T, PYCl-2 and the corresponding BHJ and SC films.

Sample	IP (100)		OOP (010)			
	q_r [Å^{-1}]	d [Å]	q_z [Å^{-1}]	d [Å]	FWHM [Å^{-1}]	L_C [Å]
PBDB-T	0.296	21.22	1.666	3.77	0.404	13.99
PYCL-2	0.345	18.20	1.634	3.84	0.321	17.60
BHJ	0.288	21.81	1.695	3.71	0.293	19.29
SC	0.292	21.51	1.637	3.84	0.310	18.23

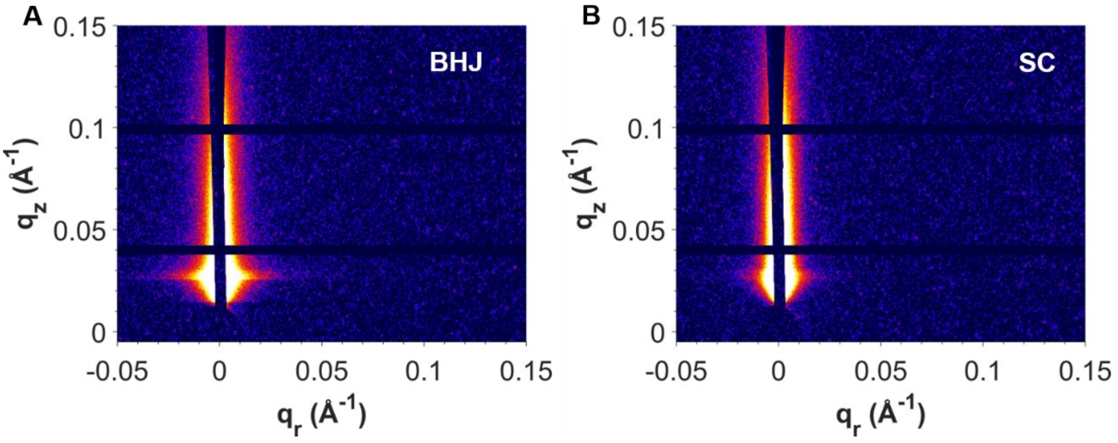

Figure S8. GISAXS patterns of the (A) BHJ and (B) SC films.

Table S5. Investigations of the domain size extracted from the GISAXS measurements of the BHJ and SC films.

Sample	In-plane domain size [nm]
BHJ	30
SC	34

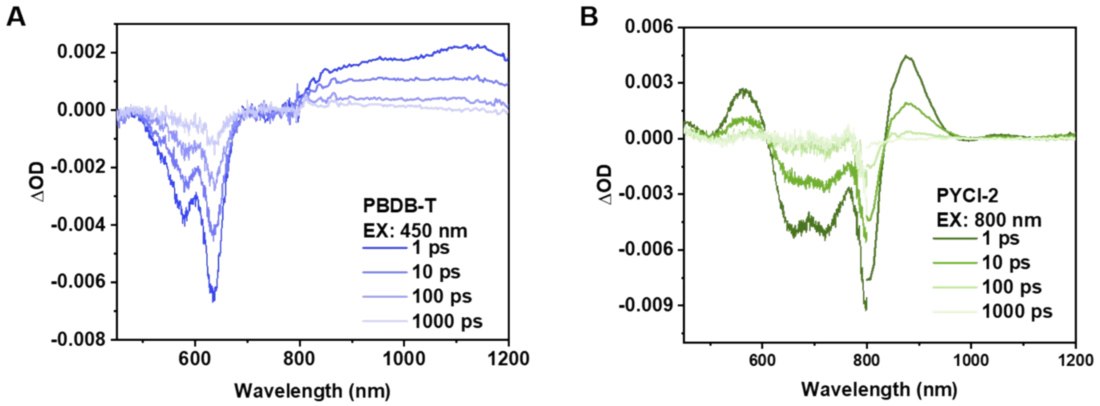

Figure S9: TA spectra of (A) the pristine PBDB-T film excited at 450 nm and (B) the pristine PYCl-2 excited at 800 nm at different delay times.

Table S6. Detailed parameters of TA spectra, the kinetics of the pristine PYCl-2 were fitted by a biexponential function: $\Delta OD(t) = A_1 exp(-t/\tau_1) + A_2 exp(-t/\tau_2)$, and the kinetics of the BHJ and SC were fitted by a multi-exponential function: $\Delta OD(t) = A_1 exp(-t/\tau_1) + A_2 exp(-t/\tau_2) + A_3 exp(-t/\tau_3)$. The films were excited at 800 nm and probed at 805 nm.

Sample	A_1	τ_1 [ps]	A_2	τ_2 [ps]	τ_{ave}[a] [ps]	N_{ED}	A_3	τ_3 [ps]
PYCl-2	5.15x10^{-3}	2.89	3.62x10^{-3}	55.96	24.80	/	/	/
BHJ	4.31x10-^{3}	1.20	2.30x10^{-3}	10.01	4.27	82.8%	1.11x10^{-3}	1237.6
SC	3.19x10^{-3}	1.47	1.75x10^{-3}	12.01	5.20	79.0%	3.63x10-^{4}	609.1

[a]The average lifetime values were calculated according to the equation: $\tau_{ave} = (A_1\tau_1 + A_2\tau_2)/(A_1 + A_2)$.

Table S7. Detailed parameters of TA spectra, the kinetics of the BHJ and SC were fitted by an exponential function: $\Delta OD(t) = A_D exp(-t/\tau_D) + B$. The films were excited at 800 nm and probed at 972 nm.

Sample	A_D	τ_D [ps]	B	N_{CD}
BHJ	6.25x10^{-4}	1260.9	1.20x10^{-3}	65.7%
SC	3.21x10^{-4}	593.2	6.19x10^{-4}	65.8%

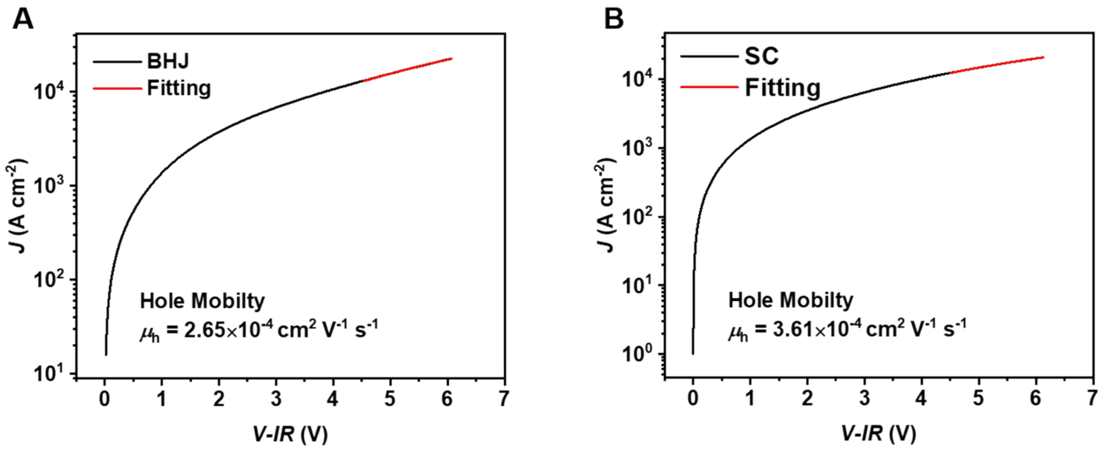

Figure S10: The dark J-V characteristics of the (A) BHJ and (B) SC based hole-only devices. The red lines represent the best fitting using the SCLC model.

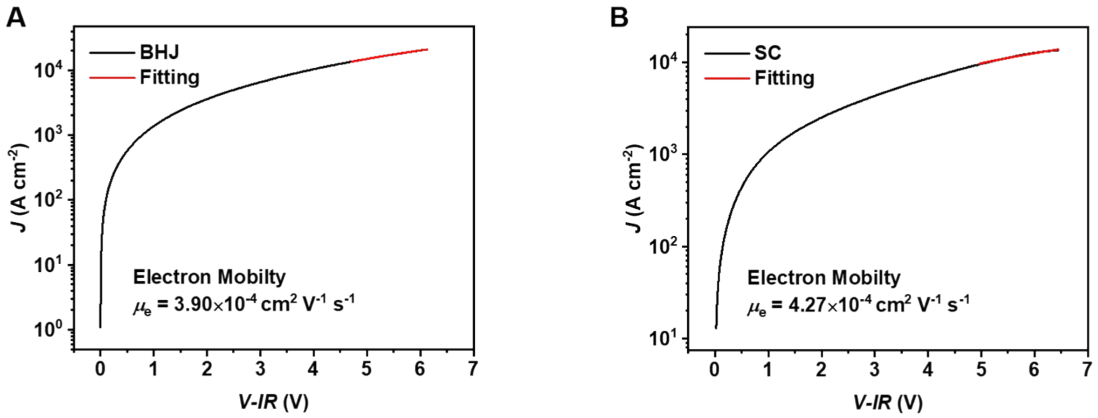

Figure S11: The dark J-V characteristics of the (A) BHJ and (B) SC based electron-only devices. The red lines represent the best fitting using the SCLC model.

Table S8. Investigations of the electron and hole mobilities and corresponding μ_h/μ_e ratios of the relevant devices extracted from the SCLC measurements.

Sample	μ_h [cm^2 V^{-1} s^{-1}]	μ_e [cm^2 V^{-1} s^{-1}]	μ_h/μ_e
BHJ	2.65×10^{-4}	3.90×10^{-4}	0.68
SC	3.61×10^{-4}	4.27×10^{-4}	0.85

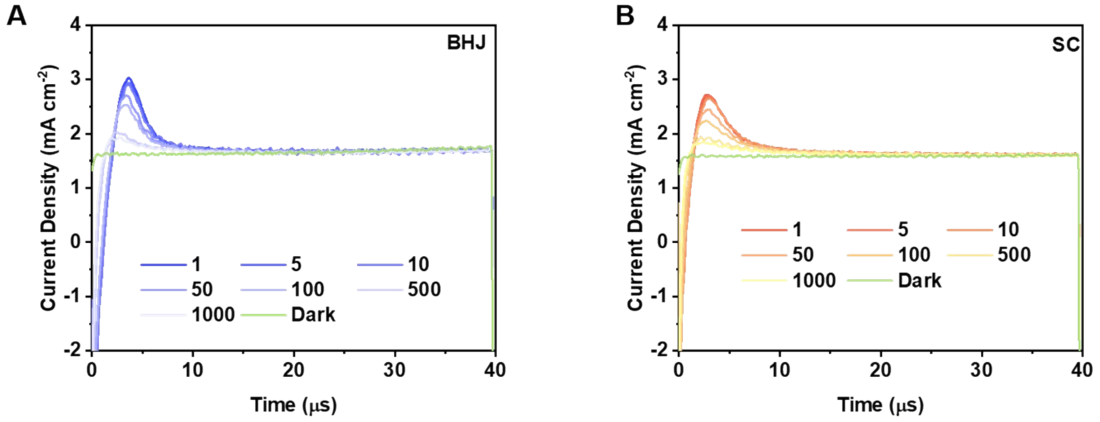

Figure S12: The photo-CELIV traces for the (A) BHJ and (B) SC devices for different delay times between the light pulse and the extraction voltage ramp.

Table S9. Parameters for calculation of the θ and α, and the diffusion length and drift length of the BHJ and SC devices.

Sample	J_{SC} [mA cm^{-2}]	V_{int} [V]	μ_h [cm^2 V^{-1} s^{-1}]	μ_e [cm^2 V^{-1} s^{-1}]	γ [cm^3 s^{-1}]	k_{rec} [s^{-1}]	k_{ex} [s^{-1}]	θ	α	l_{dif} [nm]	l_{dr} [nm]	FF [%]
BHJ	24.23	0.795	2.65x10^{-4}	3.90x10^{-4}	1.89x10^{-11}	33964.3	6.20x10^{6}	0.0439	3.22	39.4	477	68.0
SC	22.35	0.872	3.61x10^{-4}	4.27x10^{-4}	6.81x10^{-12}	7554.8	7.47x10^{6}	0.0081	1.52	57.3	1110	70.5

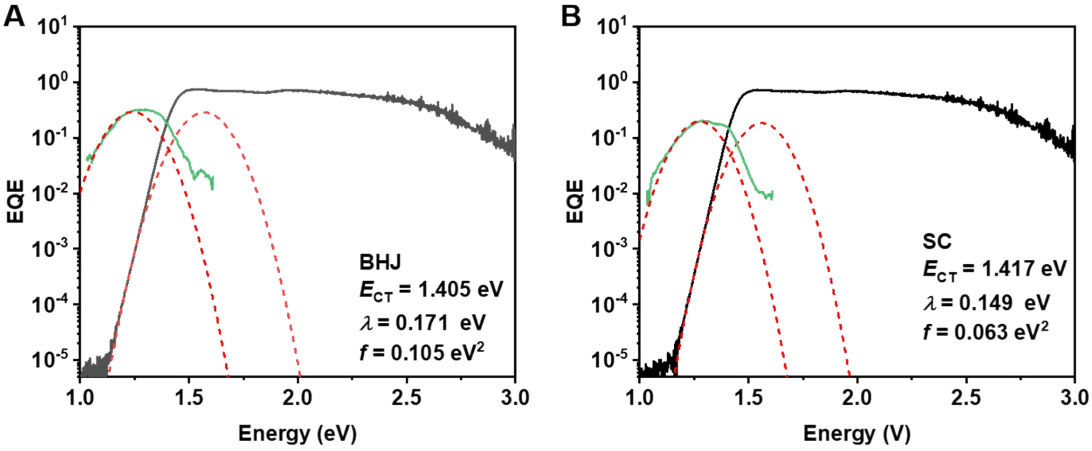

Figure S13: Fits to the FTPS-EQE and EL spectra of the (A) BHJ and (B) SC device. Values for λ, E_{CT}, and f are shown in the figure.

To estimate the reorganization energy (λ) and CT state energy (E_{CT}), we fit the FTPS-EQE tail and EL spectrum of BHJ and SC devices to the equations derived by Vandewal and coworkers[3], which describe the EL and FTPS-EQE spectra in terms of the shape and energetic position of the CT state absorption and emission spectra derived from the Marcus theory for photoinduced electron transfer[3]

$$EQE(E) = \frac{f}{E(\sqrt{4\pi\lambda k_B T})} exp(\frac{-(E_{CT}+\lambda-E)^2}{4\lambda k_B T}) \tag{4}$$

$$EL(E) = E\frac{f}{(\sqrt{4\pi\lambda k_B T})} exp(\frac{-(E_{CT}-\lambda-E)^2}{4\lambda k_B T}) \tag{5}$$

where E is the photon energy. For the fitted parameters, E_{CT} represents the free-energy difference between the charge transfer complex (CTC) ground state and the CT excited state, and E_{CT} energy can be quantified by the point of intersection between CT absorption and emission. λ is the reorganization energy associated with the CT absorption process, and f is a measure of the strength of the donor-acceptor coupling.

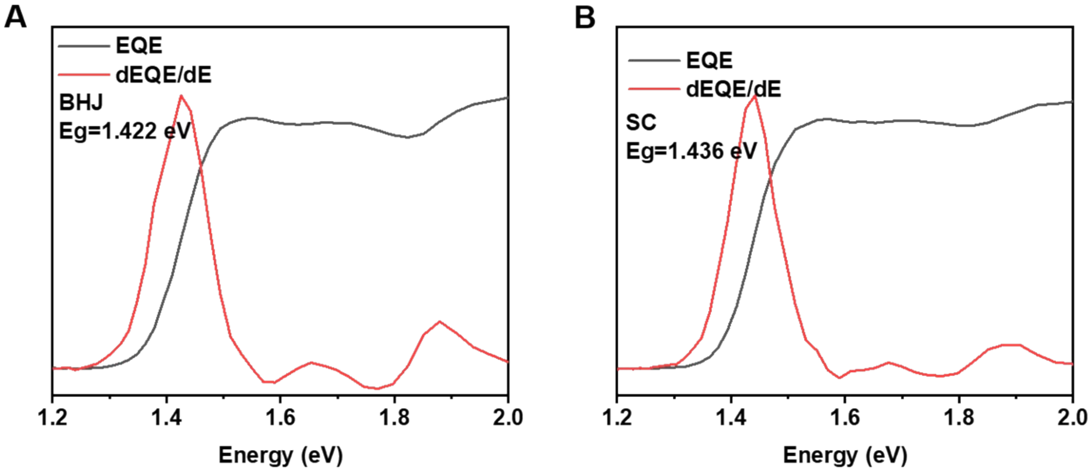

Figure S14: EQE and the its derived curves of the (A) BHJ and (B) SC devices for the calculation of the E_g^{PV}.

E_g^{PV} was determined via the method of Rau and Kirchartz,[4] and calculated by the equation of

$$E_g^{pv} = \int_a^b E_g P(E_g) dE_g / \int_a^b P(E_g) dE_g \quad , \qquad (6)$$

where $P(E_g)$ is the first derivative of the EQE_{PV} spectrum, and a and b are the FWHM limits of $P(E_g)$.

Table S10. Investigations of the different energy losses of the BHJ and SC devices extracted from the EL and FTPS measurements.

Sample	E_g^{PV} [eV]	E_{CT} [eV]	ΔV_{rad} [eV]	$\Delta V_{\mathrm{non\text{-}rad}}$ [eV]	$V_{\mathrm{OC,\ cal}}$ [V]	$V_{\mathrm{OC,\ exp}}$ [V]
BHJ	1.422	1.405	0.293	0.310	0.802	0.795
SC	1.436	1.417	0.282	0.260	0.875	0.872

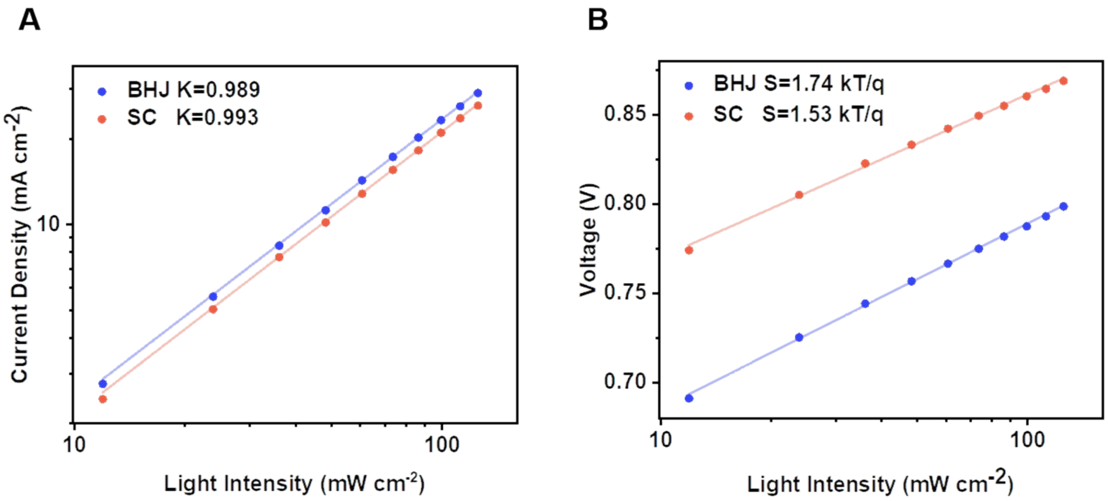

Figure S15: Light intensity dependence of (A) J_{SC} and (B) V_{OC} of the BHJ and SC devices, together with fits to the data (solid lines).

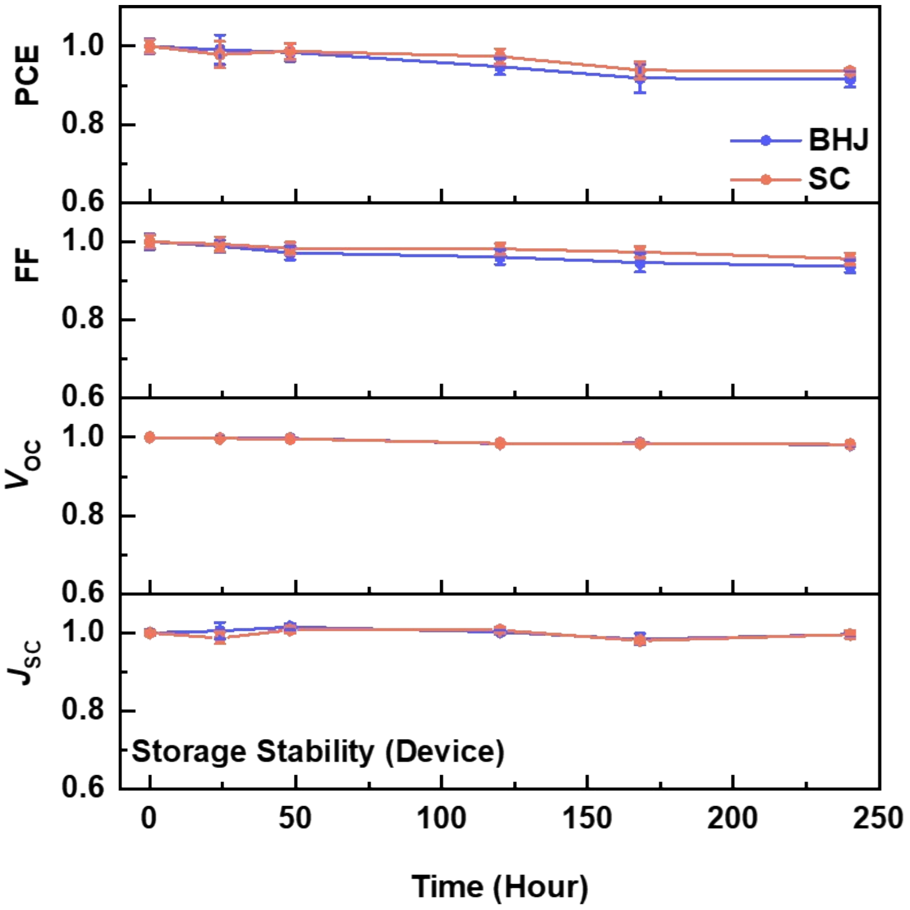

Figure S15: Degradation trends of photovoltaic parameters, including PCE, FF, V_{OC} and J_{SC} of the BHJ and SC OSCs stored in the nitrogen glovebox under the dark conditions at room temperature and measured under the illumination of AM 1.5 G at 100 mW cm^{-2}.

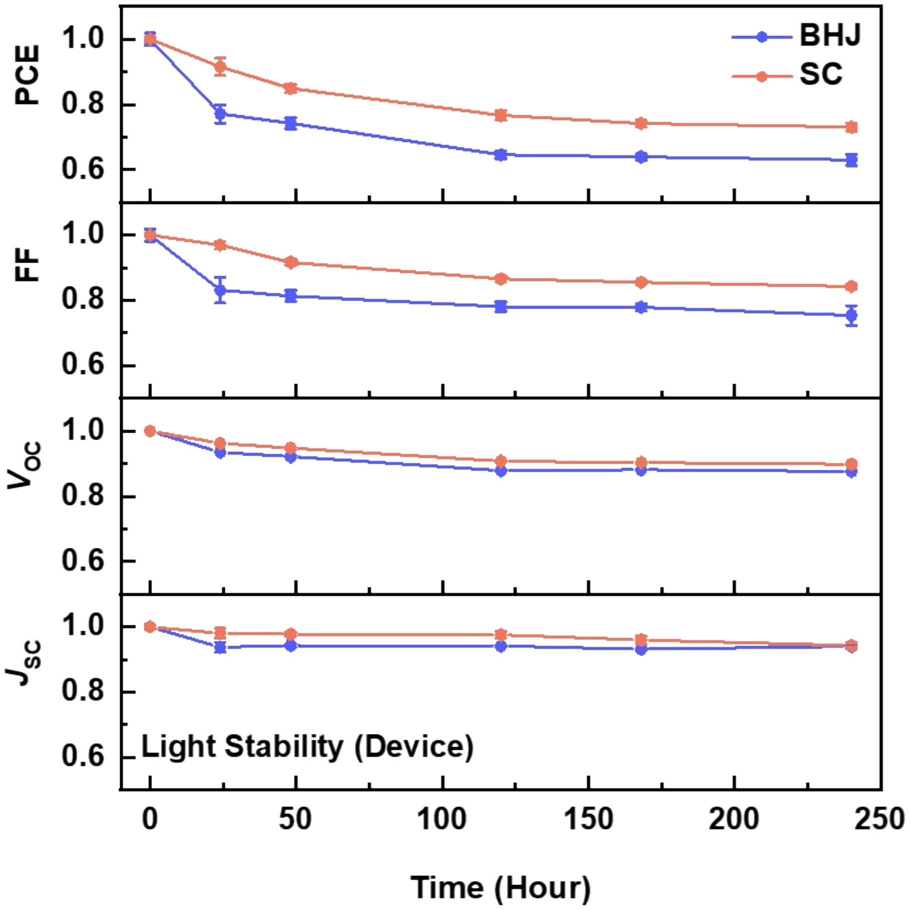

Figure S16. Degradation trends of photovoltaic parameters, including PCE, FF, V_{OC} and J_{SC} of the BHJ and SC OSCs under continuous illumination in the nitrogen glovebox at room temperature and measured under the illumination of AM 1.5 G at 100 mW cm^{-2}.

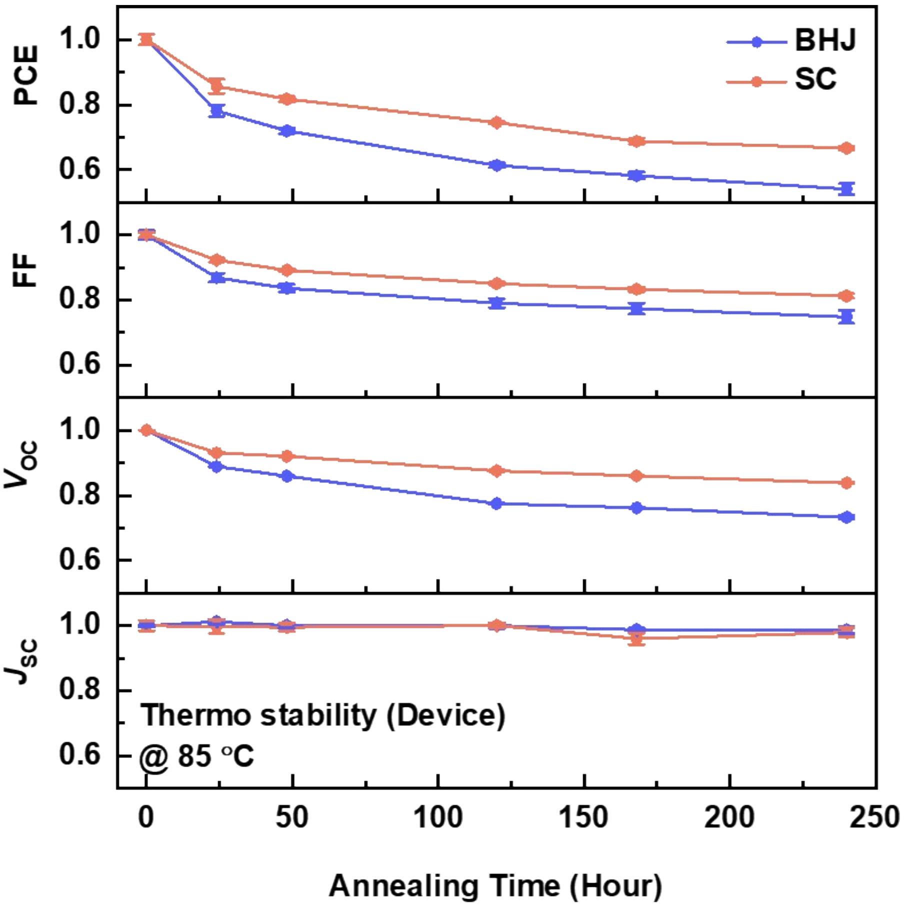

Figure S17. Degradation trends of photovoltaic parameters, including PCE, FF, V_{OC} and J_{SC} of the BHJ and SC devices annealing at 85 ℃ in the nitrogen glovebox and measured under the illumination of AM 1.5 G at 100 mW cm^{-2}.

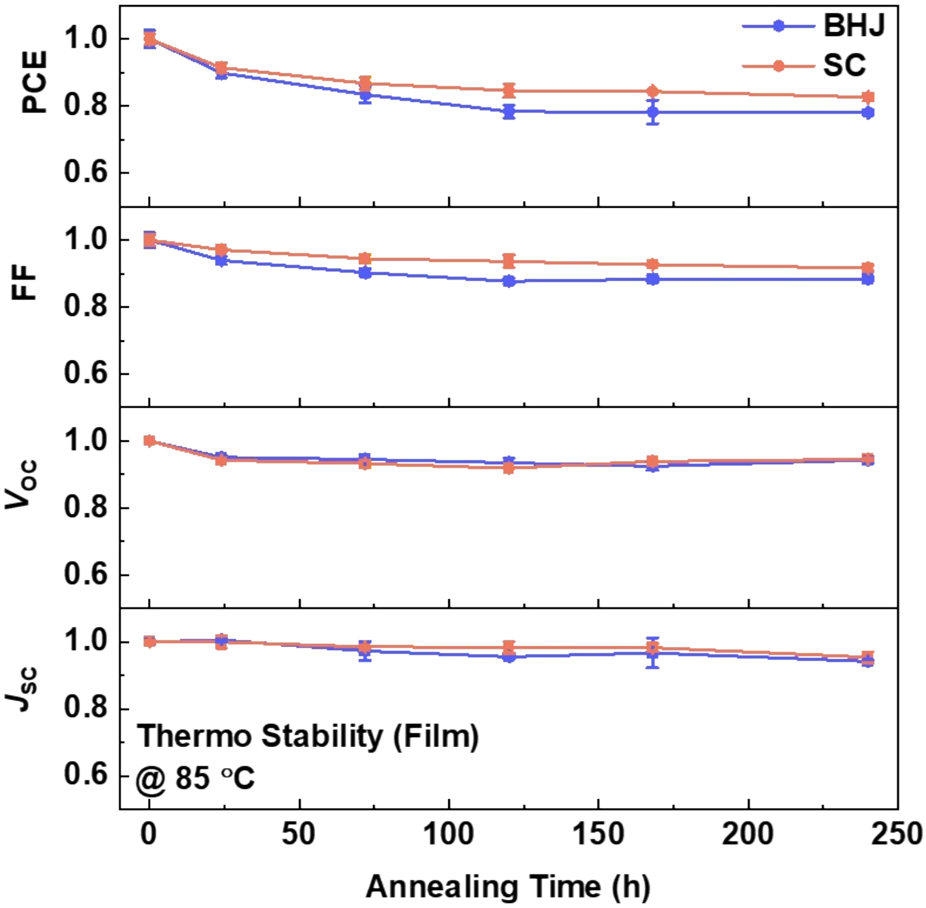

Figure S18: Degradation trends of photovoltaic parameters, including PCE, FF, V_{OC} and J_{SC} of the BHJ and SC films annealing at 85 °C in the nitrogen glovebox and measured under the illumination of AM 1.5 G at 100 mW cm^{-2}.

Reference

1. Z. Zhang, W. Si, B. Wu, W. Wang, Y. Li, W. Ma and Y. Lin, *Angew. Chem. Int. Ed.*, 2022, **61**, 202114234.
2. J. A. Carr and S. Chaudhary, *Energy Environ. Sci.*, 2013, **6**, 3414–3438.
3. K. Vandewal, K. Tvingstedt, A. Gadisa, O. Inganäs and J. V. Manca, *Phys. Rev. B*, 2010, **81**, 125204.
4. U. Rau, B. Blank, T. C. M. Müller and T. Kirchartz, *Phys. Rev. Appl.*, 2017, **7**, 044016.